



**HAL**  
open science

## **AVM nuclear glass/steel/claystone system altered by Callovo–Oxfordian poral water with and without cement–bentonite grout at 70°C**

Charly Carrière, Delphine D. Neff, Christelle Martin, Florent Tocino, Alexis Delanoë, S. Gin, Nicolas Michau, Yannick Linard, Philippe Dillmann

### ► **To cite this version:**

Charly Carrière, Delphine D. Neff, Christelle Martin, Florent Tocino, Alexis Delanoë, et al.. AVM nuclear glass/steel/claystone system altered by Callovo–Oxfordian poral water with and without cement–bentonite grout at 70°C. *Materials and Corrosion / Werkstoffe und Korrosion*, 2020, 72 (3), pp.474-482. 10.1002/maco.202011766 . cea-02910748

**HAL Id: cea-02910748**

**<https://cea.hal.science/cea-02910748>**

Submitted on 27 Aug 2020

**HAL** is a multi-disciplinary open access archive for the deposit and dissemination of scientific research documents, whether they are published or not. The documents may come from teaching and research institutions in France or abroad, or from public or private research centers.

L'archive ouverte pluridisciplinaire **HAL**, est destinée au dépôt et à la diffusion de documents scientifiques de niveau recherche, publiés ou non, émanant des établissements d'enseignement et de recherche français ou étrangers, des laboratoires publics ou privés.

## **AVM nuclear glass/steel/claystone system altered by Callovo-Oxfordian poral water with and without cement-bentonite grout at 70°C**

C. CARRIERE<sup>1</sup>, D. NEFF<sup>1</sup>, C. MARTIN<sup>2</sup>, F. TOCINO<sup>3</sup>, A. DELANOË<sup>1</sup>, S. GIN<sup>4</sup>, N. MICHAU<sup>2</sup>, Y. LINARD<sup>2</sup>, P. DILLMANN<sup>1</sup>

*1 Université Paris-Saclay, CEA, CNRS, NIMBE-LAPA, 91191 Gif-sur-Yvette Cedex, France*

*2 Andra, Research & Development Division, 1/7 rue Jean Monnet, 92298 Châtenay-Malabry, France*

*3 EDF – R&D, Département MMC, site des Renardières, 77818 Moret-sur-Loing*

*4 CEA, DEN, DE2D, University of Montpellier, Marcoule, France*

**Keywords:** AVM nuclear glass, steel corrosion, glass/steel interactions, cement-bentonite grout

### **Abstract**

The effect of a cement-bentonite grout material (CBG) was studied through glass/steel interactions. Hence 2 experimental mock-ups, consisting of a “sandwich” of 4 materials in contact: stainless-steel/AVM glass/AVM glass/P285NH steel, were leached by Callovo-Oxfordian poral water at 70°C for 1 year. CBG material was added for one experiment, whereas the second one was CBG-free. Chemical and structural analyses (SEM-EDS, Raman), performed mainly at the AVM glass/P285NH interface, evidenced a comparable alteration with and without the CBG. Indeed, its presence did not impact the gel formation by hydrolysis/condensation mechanism. For both experiments, the glass alteration rates corresponded to  $\frac{r_0^{Cox,70^\circ C}}{32}$ , highlighting a kinetic rate drop after a 1-year leaching period. However, the CBG impacted the pH solution initially buffered by the claystone, promoting precipitation of Mg/Fe-rich silicates on the gel surface. Regarding P285NH corrosion, no major difference was observed with the CBG. Steel corrosion layers in both experiments were Si-free, and the corrosion rates were similar. Therefore, after 1 year at 70°C, the CBG had a limited effect on the glass/carbon steel interactions.

## Introduction

In France, borosilicate glass was chosen to immobilize High-Level Wastes (HLW) arising from reprocessing of spent nuclear fuel, namely for its high chemical durability [1–3] and its capability to strongly bond to its structure fission products and minor actinides [4]. Those waste forms should be disposed of in a deep geological repository located in the North-East of the Parisian basin, in Callovo-Oxfordian (Cox) clay host rock [5]. To ensure the safety of populations and environment, the French National Agency for Radioactive Waste Management (Andra) has designed a multi-barriers system involving the vitrified HLW poured in a stainless-steel canister, closed in a carbon steel overpack. This waste package will be introduced into a disposal cell consisting of a horizontal microtunnel of around 0.8 m diameter with a carbon steel casing, dug into the low permeability Cox claystone, [5]. Recently, Andra planned to fill the free space between the carbon steel casing and the claystone wall of the disposal cell with a cement-bentonite grout (CBG) with a pH close to 10-11 (at 25°C) [6]. This CBG can neutralize acidity arising from oxidation reactions occurring during excavation. The aim of such a disposal design is to delay water arrival to the glass, and limit the release of radionuclides for thousands of years. Corrosion of carbon steel overpack/liner occurs before the resaturation of the disposal cell. However, the overpack failure occurs after the resaturation; it means that, after resaturation of the disposal cell, corrosion of residual steel and glass could happen. Thus, glass alteration in contact with the near-field-environment must be assessed and coupled to predictive modelling alteration over the long term.

AVM glass (produced in the Marcoule Vitrification Facility, France) is a borosilicate glass chosen to confine HLW coming from the reprocessing of Natural-Uranium Graphite Gas type fuel. Borosilicate glass performance depends on key parameters, such as temperature, water composition, and interactions between reactive materials present in the near field-environment [3,7]. According to literature, glass leaching starts with hydration/interdiffusion mechanisms [8], while water molecules penetrates the glass network (diffusivity of the order of  $10^{-20} \text{ m}^2 \cdot \text{s}^{-1}$ ). Ion-exchange then proceeds between protons and hydronium ions with alkalis acting as glass modifiers (Na, Li etc...). In parallel, hydrolysis of covalent bonds forming the glass network (Si-O-Si, Si-O-Al etc...) takes place leading to the release of orthosilicic acid in solution. As long as the concentration of Si remains low, the rate of glass alteration is maximum. This kinetic regime is called initial dissolution rate or forward rate, and the corresponding rate is noted  $r_0$ . In neutral and basic pH, dissolved Si can recondense. This mechanism leads to the formation of an amorphous hydrated layer – called gel layer – on the glass surface which become transport-limiting [9–12]. Depending on both the glass composition and the solution composition, such a layer can form by dissolution/reprecipitation or by in-situ recondensation of incompletely detached Si species [13–16]. However presence of other materials could modify

chemical equilibria and affect the passivating properties of the gel. For example, iron ions in solution brought from steel corrosion can precipitate preferentially with hydrolysed Si to form Fe-Si-O phases, preventing the formation of a dense gel layer. Indeed such secondary phases were already evidenced in glass alteration experiments [17–19]. The presence of CBG could shift the pH to a higher value than that in equilibrium with the Cox claystone and this should increase the solubility of the gel [20]. The consequence are difficult to predict [21].

To the best of our knowledge, no laboratory experiment has focused on AVM glass alteration, in presence of steel and claystone. Moreover, influence of the CBG material on a joint glass/steel alteration has not been investigated. This paper reports results from two mock-up experiments allowing us to better understand how glass behave in these complex systems. Two AVM simulant glass/carbon steel/claystone systems were interacting in the presence of Cox synthetic groundwater for one year at 70 °C. CBG material was added for one system, whereas the second one was CBG-free. This study focuses on the influence of the CBG material, on the AVM glass and carbon steel interactions. Hence interface between the glass and the carbon steel is observed at the micrometer scale (SEM-EDS,  $\mu$ Raman spectroscopy) for both systems, and the influence of the CBG material is discussed throughout the study.

## Materials and methods

### AVM glass/steel/claystone systems

Two glass/steel/claystone systems were altered in contact with synthetic representative Cox poral water, with and without the CBG. The non-radioactive AVM V4 nuclear glass was chosen for this study (composition given in Table 1). It presents an average composition of all AVM glasses, and is referenced as the representative AVM glass [22]. The first system consisted of a “sandwich” of four roughly polished sections (about 25 mm × 25 mm × 2 mm thick) pressed and in contact: 309 stainless-steel/AVM glass2/AVM glass1/P285NH carbon steel (composition of the carbon steel given in Table 2). Thickness of the water film between these sections was of the order of magnitude of their roughness. The “sandwich” was placed in a stainless-steel reactor containing Cox claystone recovered from the Andra’s Underground Research laboratory. Then reactor was arranged vertically and the system was saturated by a synthetic Cox groundwater (composition in Table 3), with a water circulation from bottom to top. Saturation was performed at an adapted flow rate using a peristaltic pump. The Figure 1 presents a schematic view of the alteration experiment. The second system was similar to the first one, but the cement-bentonite grout (CBG) material was added around the “sandwich” of the four sections (Figure 1). CBG was mainly composed of cement CEMIII and bentonite and the water to solid phases mass ratio (w/s) was close to 3 (composition of the CBG in Table 4). Note that the mass ratio

CBG/Cox claystone corresponded to 1/100. The two systems were altered under anoxic and carbonated medium in two different reactors at 70°C for 1 year.

After alteration, the claystone cores containing the samples were taken out of the reactors and were embedded in a bi-component epoxy resin (resin + hardener). Note that it was not possible to take any measure to avoid a possible oxidation. Then transverse sections were cut and samples were mechanically polished with SiC paper (500, 800, 1200, 2400, 4000) under ethanol followed by 3 µm and 1 µm polishing using diamond suspension. Finally, samples were ultrasonically cleaned for 3 min in acetone and 3 min in ethanol.

## Analytical techniques

### SEM-EDS

Scanning electron microscopy coupled with dispersive energy spectroscopy (SEM-EDS) was used to observe the alteration at the AVM glass 1/P285NH steel interface on both systems. To avoid charge accumulation on the glass surface, samples were coated with a carbon layer of 15 nm thick. Analyses were conducted using a Jeol JSM-7001F Field Effect Scanning Electron Microscope (SEM-FEG) coupled to an EDS SDD detector (Silicon Drift Detector) for chemical analysis. The incident acceleration voltage of 15 kV was chosen to excite all the characteristic lines of the elements of interest.

### MicroRaman spectroscopy

µRaman analyzes were performed at the same interface of the samples on an Invia Renishaw micro-spectrometer equipped with a Nd-YAG green laser doubled with 532 nm wavelength, with a CCD detector associated with a 2400-line array. Laser power was filtered at 0.1 mW. The beam was focused using a Leica DMLM optical microscope with a ×50 lens. The size of the beam was approximately 1 µm<sup>2</sup>. Raman spectra were recorded with a resolution of 2 cm<sup>-1</sup> and the spectrometer was calibrated on a silicon wafer with a main vibration band at 520.5 cm<sup>-1</sup>. Wire 3.4 software was used for all spectra acquisition in point mode.

## Results and discussion

### AVM glass/steel/claystone without the CBG environment

The aim of the study concerns the influence of the CBG material on the glass/steel interactions, that is why results presented here were performed only at the AVM glass 1/P285NH interface. As a reminder, the 4 plates of glass and steel were in contact during alteration, and the initial pH solution was close to 7. SEM-EDS analyses (Figure 2, Table 5) show the glass and P285NH steel alteration facies observed in the sample. In particular, an alteration layer, named gel, of 5 µm thick ( $\sigma = 0.5 \mu\text{m}$ , about 10

measurements) and depleted in Na is observed along the pristine glass (PG). While Na is present in large quantity in the PG (13 wt.%), the gel contains only 2 wt.% of it, due to ion-exchange reactions [8,23]. Al and Mg are also detected in the gel, with contents close to those of the PG. Furthermore, the gel seems to be enriched in Si (32 wt.%) versus the PG (23 wt.%). However in PG and gel of the AVM glass, the total content of Si+Al+Na = 43% and remains constant [19], as evidenced in Table 5. Therefore, due to the release of Na, the EDS semi-quantitative analyses suggest that the Si content does not vary significantly between PG and gel. The resulting high retention of Si is consistent with the formation of a gel in a confined and low reactive environment. Interestingly, the gel is not enriched in Fe, while steel corrodes at the same time nearby the glass (see below). Indeed, close to neutral pH, literature evidences Fe penetration in the gel when SON68 glass [24,25], ISG glass [26], or archeological glass [27,28] are leached near an iron source.

Facing the glass, an iron corrosion product layer is formed on the metal surface. SEM micrograph (in backscattered electron mode) and the EDS distribution maps of oxygen and iron (Figure 2) evidence a uniform corrosion layer of 4  $\mu\text{m}$  thick ( $\sigma = 0.5$ , 10 measurements). Iron corrosion products (ICP) were identified by  $\mu\text{Raman}$  spectroscopy (Figure 3). Spectra obtained in the system studied here, corresponding to the spectrum in grey, have an intense vibration band at  $1084\text{ cm}^{-1}$ , and three less intense bands at  $287$ ,  $396$  and  $744\text{ cm}^{-1}$ . These bands are characteristic of a precipitated iron carbonate, the siderite  $\text{FeCO}_3$ , a typical ICP in carbonated environment [29,30]. Hence the average corrosion rate can be estimated with a method based of the Pilling-Bedworth ratio (PBR), taking into account the volume expansion of the ICP layer versus the pristine metal. With a  $\text{PBR} = 4.2$  for the siderite [31], the corrosion rate corresponds to  $0.95\text{ }\mu\text{m}\cdot\text{year}^{-1}$ , in good agreement with the ones observed for a carbon steel corroded in an anoxic and/or carbonated environment [32–34]. This calculation assumes that all corroded Fe precipitates in ICP. However, in saturated clay media, only half of oxidized Fe is retained and the other part is potentially transported elsewhere [35]. Therefore corrosion rate in the system studied here could be higher, about  $1.9\text{ }\mu\text{m}\cdot\text{year}^{-1}$ . Regarding chemical composition of ICP (Table 5), no Si (less than 1 wt.%) was detected, contrary to a similar previous study with the same “sandwich” of 4 materials [36]. Nevertheless, it was a study involving 2 SON68 glass plates and 2 steel plates (stainless steel and P285NH) altered at  $90\text{ }^\circ\text{C}$  without CBG.

To summarize, in the sample investigated here, a non-Si depleted gel is formed on the PG surface. No Fe migration was observed in the gel of  $5\text{ }\mu\text{m}$  thick, and Si was not detected in ICP. Therefore, after 1 year of leaching at  $70^\circ\text{C}$  in a solution buffered by the Cox, both iron and AVM glass altered without showing any steel/glass interactions. AVM glass does not seem impacted by the presence of iron.

## AVM glass/steel/claystone in the presence of CBG

The effect of CBG, located between the “sandwich” and claystone, was investigated in a similar AVM glass/steel/claystone system altered under the same conditions. Along the PG, a gel of 5  $\mu\text{m}$  thick ( $\sigma = 1 \mu\text{m}$ , about 10 measurements), can be identified from the Na depleted zone (Figure 4 and Table 5). As previously observed, the gel contains Al and Mg with amounts close to the PG, and is not enriched in Fe. During alteration, the Si was retained in the gel for the same reason explained before. However, with the CBG, SEM-EDS analyses revealed precipitated aggregates along the gel surface (Figure 4). In most cases, they contain mostly Si (32 wt.%), Mg (13 wt.%), Al (8 wt.%) and O (43 wt.%), and minor elements such as Ca (2 wt.%) and Fe (1.4 wt.%), as shown in Figure 4-a and Table 6. These constituents correspond to those already observed in phyllosilicates formed during AVM glass alteration in solution containing Mg only [37]. Besides, the author unambiguously identified these Si-Mg-Al phases as trioctahedral smectite (saponite), with a Mg(II)-rich octahedral layer and an Al distribution in both octahedron and tetrahedron sites. However further precipitated phases were observed in the study presented here. Figure 4-b evidences two phases containing Fe, mostly constituted with Si-Fe-Ca-O or Ca-Fe-O (Table 6). The first one could correspond to an Fe-rich phyllosilicate already observed in nuclear glass/iron interactions studies [25,38–40], while the second one seems to be an iron carbonate. Note that these phases were not successfully identified by  $\mu\text{Raman}$  spectroscopy, probably because of their poor crystallinity and/or low Raman scattering.

The steel facing the glass is corroded and presents the same corrosion facies than the system without CBG (Figure 4). Indeed, the corrosion layer of 4  $\mu\text{m}$  thick ( $\sigma = 1 \mu\text{m}$ , 10 measurements), and the composition (Table 5) are identical.  $\mu\text{Raman}$  analyses (Figure 3) assimilate ICP as chukanovite,  $\text{Fe}_2(\text{OH})_2\text{CO}_3$ , a precipitated Fe-carbonate, with an intense vibration band at  $1070 \text{ cm}^{-1}$ , and two less intense bands at  $391$  and  $728 \text{ cm}^{-1}$  on the spectra [30]. As well as the system without CBG, the average corrosion rate with CBG is  $1 \mu\text{m}\cdot\text{year}^{-1}$  (PBR of chukanovite = 4.0 [31]), but could be doubled as explained before.

Therefore, in the two systems (with and without CBG) glass and steel shares common features. The Fe-free gels do not seem depleted in Si. As a gel growth is generally described as isovolumetric [41,42], the glass alteration rates in both systems can be determined using the gel thickness. Assuming a constant alteration rate, they are similar and correspond to  $3.4 \cdot 10^{-2} \text{ g}\cdot\text{m}^{-2}\cdot\text{day}^{-1}$  (using an AVM glass density equal to  $2.5 \text{ g}\cdot\text{cm}^{-3}$  [22]). The presence of Mg-rich and/or Fe-rich silicate on the gel surface was detected only in the system containing CBG. These phases could be assimilated to smectite. However, at this stage, it is not possible to determine the origin of the Si contained in the silicates (glass or Cox solution). But considering the Si retention in the gel, the silicates certainly precipitated mainly with the Si contained in the Cox solution [43], using the Mg released by glass alteration. Regarding ICP, no major

difference was observed. They correspond to an Si-free iron carbonate, and the corrosion rates are similar.

### Influence of the CBG environment on glass/steel/claystone interactions

The influence of the CBG, located between the “sandwich” and claystone, was assessed regarding the glass/steel interactions, through 2 systems aged in the same conditions (70 °C, one year). In the CBG-free system, the leached solution is buffered by the Cox claystone, close to neutrality [44]. However, in presence of a cement material, the pH of the solution could be higher, as the CBG pore solution pH reaches 10-11. Such a pH could impact glass/steel interactions.

Concerning glass alteration, a gel of 5 µm thick is observed on the PG surface with and without CBG. The associated alteration rate is  $3.4 \cdot 10^{-2} \text{ g} \cdot \text{m}^{-2} \cdot \text{day}^{-1}$ , for both systems. To our knowledge, no AVM glass alteration experiments were performed in Cox water at 70 °C, and/or in presence of an iron source. However a preliminary study evidenced an initial dissolution rate of AVM V4 at  $r_0^{\text{Cox}, 50^\circ\text{C}} = 2.4 \cdot 10^{-1} \text{ g} \cdot \text{m}^{-2} \cdot \text{day}^{-1}$  obtained in Cox water at 50°C, without an iron source (Nicole Godon, unpublished data). To compare our values to an initial dissolution rate at the same temperature, the activation energy ( $Ea$ ) associated to  $r_0^{\text{Cox}}$ , can be calculated using the expression of the initial dissolution rate  $r_0$  in Equation 1 [7]:

$$r_0^{\text{Cox}} = k^+ a_{\text{H}^+}^n e^{-\frac{Ea}{RT}} \left(1 - \frac{a_{\text{H}_4\text{SiO}_4}}{K}\right)$$

**Equation 1:**

$k^+ = 1.2 \cdot 10^8 \text{ g} \cdot \text{m}^{-2} \cdot \text{d}^{-1}$  is the kinetic constant,  $n = -0.4$  the coefficient of the pH-dependence of the reaction rate.

With an  $a_{\text{H}_4\text{SiO}_4} = 0$  in solution (no Si released in solution), the  $Ea$  equals  $70.9 \text{ kJ} \cdot \text{mol}^{-1}$ , consistent with the apparent activation energy of initial rate calculated at  $76 \text{ kJ} \cdot \text{mol}^{-1}$  ( $\sigma = 5 \text{ kJ} \cdot \text{mol}^{-1}$ ) by Frugier et al. [7]. Hence, at 70 °C, the  $r_0^{\text{Cox}, 70^\circ\text{C}}$  of AVM V4 glass corresponds presumably to  $1.1 \text{ g} \cdot \text{m}^{-2} \cdot \text{day}^{-1}$ . In the study presented here, the AVM glass alteration of both systems ( $3.4 \cdot 10^{-2} \text{ g} \cdot \text{m}^{-2} \cdot \text{day}^{-1}$ ) is significantly lower than  $r_0^{\text{Cox}}$ , i.e.  $\frac{r_0^{\text{Cox}}}{32}$ . This value probably highlights a passivating and protective behavior of the gel. Indeed, such a gel could be formed by Si recondensation, which tends to increase its density and diminish its porosity and therefore the silica diffusion coefficient [45,46]. Indeed, the condensation and the densification of the gel can clog the porosity, and the gel could act as a diffusive barrier that limits exchanges at the gel/solution interface [14,47]. It could also explain that no Fe was incorporated into the gel porosity, although steel corrosion occurred simultaneously. Besides, presence of Mg in

such AVM glass composition reinforces the passivating properties of the gel as it was demonstrated by Thien et al. [19].

The only differences between the two altered systems concerns presence of chukanovite in ICP layer rather than siderite, and precipitated Mg-rich and Fe-rich silicates at the gel surface, with the CBG. Regarding steel corrosion in an anoxic and carbonated environment, chukanovite formation is promoted in alkaline conditions [48]. Furthermore, the Mg-rich phases could correspond to saponite, a trioctahedral smectite already identified by other studies in AVM glass leaching experiments [19,37]. These authors associate this phase as a Si pump, which consumes the Si from the gel leading to a less protective gel. However, regarding to the gel thickness and the dissolution rates of our two experiments, the silicates present with the CBG seem harmless for the glass alteration. The Si in silicate probably comes mainly from the Cox solution. Nevertheless, the CBG affects the pH of the solution. Indeed, Mg-rich smectites are preferentially formed at higher pH, close to 8 or 9 [26,49], which indicates a pH increasing of the leaching solution with the CBG. Fe-rich silicates were also identified with the CBG, highlighting glass/steel interaction through Fe/Si affinity. In the case of Fe-rich smectites, the more iron there is, the lower the solubility is (Table 7), which may explain a preferential precipitation of Fe-rich phases when an iron source is present in solution. But whatever the identified silicate, smectite precipitation leads to a local pH decrease [19,50], while glass dissolution increases it by releasing alkali elements, i.e. sodium and boron in solution [51–53]. Hence local and cyclic pH modifications could occur near the gel reaching a steady-state, unaffected the latter, and promoting silicate precipitation at the vicinity of the glass.

Therefore, the CBG seems to have a limited effect on the glass alteration mechanisms and iron corrosion at the AVM glass/P285NH interface. After one year at 70°C, the CBG would not prevent a passive gel formation by hydrolysis/condensation, and would not modify significantly the generalized corrosion behavior.

## Conclusions

Two glass/steel/claystone systems were leached with Cox groundwater for one year at 70 °C in laboratory, with or without the cement-bentonite grout. The effect of this material, located between the “sandwich” and claystone, was investigated through glass/steel interactions. His presence has a limited effect on the glass alteration facies, and does not impact the gel formation by hydrolysis/condensation mechanism observed in the two systems. After one year, the glass alteration rates calculated on both systems are lower than the initial dissolution rate, corresponding to  $\frac{r_0^{Cox,70^\circ C}}{32}$ .

This rate drop is probably the result of the dense and protective gel, which limits exchanges between the glass and the solution. Nevertheless, the CBG modifies the pH solution initially buffered by the Cox claystone, promoting precipitation on the gel surface of Mg-rich and/or Fe-rich silicates, presumably assimilated as smectites. Regarding carbon steel corrosion, no major difference was observed with the CBG. In both systems, the corrosion layer is Si-free, and the corrosion rate is about  $2 \mu\text{m}\cdot\text{year}^{-1}$ . After one year at  $70^\circ\text{C}$ , neither carbon steel nor CBG affect the AVM V4 glass. These observations could reinforce the understanding of glass/steel/claystone interaction necessary to model the waste package behavior on the long term.

## References

- [1] M.I. Ojovan, W.E. Lee, *New developments in glassy nuclear wasteforms*, Nova Publishers, New York, **2007**.
- [2] I.W. Donald, *Waste immobilization in glass and ceramic based hosts: radioactive, toxic, and hazardous wastes*, John Wiley & Sons, Chichester, **2010**.
- [3] B. Grambow, *Elements*. **2006**, 2, 357–364.
- [4] S. Gin, P. Jollivet, M. Tribet, S. Peugeot, S. Schuller, *Radiochim. Acta*. **2017**, 105, 927–959.
- [5] ANDRA, *Evaluation of the feasibility of a geological repository in an argillaceous formation*, **2005**.
- [6] M. Robineau, A. Romaine, R. Sabot, M. Jeannin, V. Deydier, S. Necib, P. Refait, *Electrochim. Acta*. **2017**, 255, 274–285.
- [7] P. Frugier, S. Gin, Y. Minet, T. Chave, B. Bonin, N. Godon, J.-E. Lartigue, P. Jollivet, A. Ayrat, L. De Windt, G. Santarini, *J. Nucl. Mater.* **2008**, 380, 8–21.
- [8] B.C. Bunker, G.W. Arnold, D.E. Day, P.J. Bray, *J. Non. Cryst. Solids*. **1986**, 87, 226–253.
- [9] D. Rebiscoul, A. Van der Lee, F. Rieutord, F. Né, O. Spalla, A. El-Mansouri, P. Frugier, A. Ayrat, S. Gin, *J. Nucl. Mater.* **2004**, 326, 9–18.
- [10] S. Gin, A. Abdelouas, L.J. Criscenti, W.L. Ebert, K. Ferrand, T. Geisler, M.T. Harrison, Y. Inagaki, S. Mitsui, K.T. Mueller, *Mater. Today*. **2013**, 16, 243–248.
- [11] J.D. Vienna, J. V Ryan, S. Gin, Y. Inagaki, *Int. J. Appl. Glas. Sci.* **2013**, 4, 283–294.
- [12] C. Cailleteau, F. Angeli, F. Devreux, S. Gin, J. Jestin, P. Jollivet, O. Spalla, *Nat. Mater.* **2008**, 7, 978.
- [13] R. Hellmann, S. Cotte, E. Cadel, S. Malladi, L.S. Karlsson, S. Lozano-Perez, M. Cabié, A. Seyeux, *Nat. Mater.* **2015**, 14, 307.
- [14] S. Gin, P. Jollivet, M. Fournier, F. Angeli, P. Frugier, T. Charpentier, *Nat. Commun.* **2015**, 6, 6360.
- [15] S. Gin, M. Collin, P. Jollivet, M. Fournier, Y. Minet, L. Dupuy, T. Mahadevan, S. Kerisit, J. Du, *Nat. Commun.* **2018**, 9, 2169.
- [16] S. Gin, A.H. Mir, A. Jan, J.-M. Delaye, E. Chauvet, Y. De Puydt, A. Gourgiotis, S.N. Kerisit, *J. Phys. Chem. C*. **2020**, 124, 9, 5132-5144.
- [17] E. Curti, J.L. Crovisier, G. Morvan, A.M. Karpoff, *Appl. Geochemistry*. **2006**, 21, 1152–1168.
- [18] P. Frugier, C. Martin, I. Ribet, T. Advocat, S. Gin, *J. Nucl. Mater.* **2005**, 346, 194–207.
- [19] B.M.J. Thien, N. Godon, A. Ballesterro, S. Gin, A. Ayrat, *J. Nucl. Mater.* **2012**, 427, 297–310.
- [20] K.R. Iler, *The chemistry of silica, Solubility*, *Polym. Colloid Surf. Prop. Biochem. Silica*. **1979**.
- [21] M. Fournier, T. Ducasse, A. Pérez, A. Barchouchi, D. Daval, S. Gin, *J. Nucl. Mater.* **2019**, 524, 21-38.
- [22] S. Narayanasamy, *Ph.D. Thesis*, Ecole Nationale Supérieure Mines-Telecom Atlantique Bretagne Pays de la Loire, France, **2019**.

- [23] E.Y. Vernaz, J.L. Dussossoy, *Appl. Geochemistry*. **1992**, 7, 713–22.
- [24] D. Rébiscoul, E. Burger, F. Bruguier, N. Godon, J.-L. Chouchan, J.-P. Mestre, P. Frugier, J.-E. Lartigue, S. Gin, *MRS Proc.* **2013**, 1518, 185–190.
- [25] P. Dillmann, S. Gin, D. Neff, L. Gentaz, D. Rebiscoul, *Geochim. Cosmochim. Acta.* **2016**, 172, 287–305.
- [26] H. Aréna, N. Godon, D. Rébiscoul, P. Frugier, R. Podor, E. Garcès, M. Cabie, J.-P. Mestre, *Appl. Geochemistry*. **2017**, 82, 119–133.
- [27] A. Michelin, E. Burger, E. Leroy, E. Foy, D. Neff, K. Benzerara, P. Dillmann, S. Gin, *Corros. Sci.* **2013**, 76, 403–414.
- [28] H.G. Changela, J.C. Bridges, *Meteorit. Planet. Sci.* **2010**, 45, 1847–1867.
- [29] M.L. Schlegel, C. Martin, F. Brucker, C. Bataillon, C. Blanc, M. Chorro, P. Jollivet, *Appl. Geochemistry*. **2016**, 70, 27–42.
- [30] M. Saheb, D. Neff, L. Bellot-Gurlet, P. Dillmann, *J. Raman Spectrosc.* **2011**, 42, 1100–1108.
- [31] M. Saheb, *Ph.D. Thesis*, Université Paris-Est, France, **2009**.
- [32] N. Taniguchi, presented at EUROCORR'04, Nice, France, **2004**, pp. 24–34.
- [33] J. Jelinek, P. Neufeld, *Corrosion*. **1982**, 38, 98–104.
- [34] N.R. Smart, D.J. Blackwood, L. Werme, *The anaerobic corrosion of carbon steel and cast iron in artificial groundwaters*, Swedish Nuclear Fuel and Waste Management Co., **2001**.
- [35] M.L. Schlegel, C. Bataillon, C. Blanc, D. Prêt, E. Foy, *Environ. Sci. Technol.* **2010**, 44, 1503–1508.
- [36] C. Carrière, F. Mercier, M. Bouttemy, E. Foy, X. Crozes, A. Etcheberry, D. Neff, I. Monnet, P. Dillmann, *J. Electron Spectros. Relat. Phenomena.* **2019**, 235, 51–59.
- [37] B. Thien, N. Godon, F. Hubert, F. Angéli, S. Gin, A. Ayral, *Appl. Clay Sci.* **2010**, 49, 135–141.
- [38] G. De Combarieu, M.L. Schlegel, D. Neff, E. Foy, D. Vantelon, P. Barboux, S. Gin, *Appl. Geochemistry*. **2011**, 26, 65–79.
- [39] M.L. Schlegel, C. Bataillon, K. Benhamida, C. Blanc, D. Menut, J.-L. Lacour, *Appl. Geochemistry*. **2008**, 23, 2619–2633.
- [40] E. Burger, D. Rebiscoul, F. Bruguier, M. Jublot, J.E. Lartigue, S. Gin, *Appl. Geochemistry*. **2013**, 31, 159–170.
- [41] N. Donzel, S. Gin, F. Augereau, M. Ramonda, *J. Nucl. Mater.* **2003**, 317, 83–92.
- [42] J.T. Reiser, B. Parruzot, M.H. Weber, J. V Ryan, J.S. McCloy, N.A. Wall, *J. Nucl. Mater.* **2017**, 490, 75–84.
- [43] C. Carrière, *Ph.D. Thesis*, Université Pierre et Marie Curie – Sorbonne Université, France, **2017**.
- [44] A. Vinsot, S. Mettler, S. Wechner, *Phys. Chem. Earth, Parts A/B/C.* **2008**, 33, Supple, S75–S86.
- [45] O. Zarembowitch-Deruelle, *Ph.D. Thesis*, Université Pierre et Marie Curie, France, **1997**.
- [46] E. Vernaz, S. Gin, C. Jégou, I. Ribet, *J. Nucl. Mater.* **2001**, 298, 27–36.

- [47] P. Jollivet, F. Angeli, C. Cailleteau, F. Devreux, P. Frugier, S. Gin, *J. Non. Cryst. Solids*. **2008**, 354, 4952–4958.
- [48] I. Azoulay, C. Rémazeilles, P. Refait, *Corros. Sci.* **2012**, 58, 229–236.
- [49] V.C. Farmer, G.S.R. Krishnamurti, P.M. HtJANG, *Clays Clay Miner.* **1991**, 39, 561–570.
- [50] J.C. Fernández-Caliani, E. Crespo, M. Rodas, J.F. Barrenechea, F.J. Luque, *Clays Clay Miner.* **2004**, 52, 106–114.
- [51] Y. Wang, C.F. Jove-Colon, K.L. Kuhlman, *Sci. Rep.* **2016**, 6, 30256.
- [52] S. Ribet, S. Gin, *J. Nucl. Mater.* **2004**, 324, 152–164.
- [53] H. Aréna, N. Godon, D. Rébiscoul, R. Podor, E. Garcès, M. Cabie, J.P. Mestre, *J. Nucl. Mater.* **2016**, 470, 55–67.
- [54] N. Michau, X. Bourbon, French Patent, 3 031 103, **2014**.
- [55] C.M. Bethke, B. Farrell, S. Yeakel, *The Geochemist's Workbench*, Version 12.0: *GWB Essentials Guide*. Aqueous Solutions, LLC, Champaign, Illinois, US., **2018**.
- [56] J.C. Wilson, S. Benbow, H. Sasamoto, D. Savage, C. Watson, *Appl. Geochemistry*. **2015**, 61, 10–28.

## Tables

**Table 1: composition of AVM V4 glass (wt.%)**

Oxides	SiO <sub>2</sub>	B <sub>2</sub> O <sub>3</sub>	Na <sub>2</sub> O	Al <sub>2</sub> O <sub>3</sub>	MgO	Fe <sub>2</sub> O <sub>3</sub>	F	other
AVM V4	43.37	17.43	17.28	10.92	4.32	0.90	0.72	rest

**Table 2: composition of the steel P285NH (wt.%)**

Element	C	Si	Mn	Ni	Cr	Cu	others	Fe
EN 10222-4	0.18	0.4	0.6-1.5	0.3 max	0.3 max	0.2 max	0.29 max	rest

**Table 3: chemical composition of the synthetic Cox groundwater**

	Na	K	Ca	Mg	Sr	Si	Cl	SO <sub>4</sub>	HCO <sub>3</sub>	Eh vs. SHE	pH
mg/L	966	39.1	397	99.6	17.5	9.8	1453	1345	232	-0.14 V	6.86

**Table 4: chemical composition of the CBG [54]**

constituents	quantity (kg/m <sup>3</sup> )
Cement CEM III/C 32,5 N SR CE PM NF	126
Silica fume	126
bentonite	33.6
hydrotalcite	8.4
water	881

**Table 5: SEM-EDS chemical composition analysis (wt.%) of the gel, PG, and ICP obtained in rectangular areas shown on figure 2 and 4 (n.d. not detected)**

Elements	O	Si	Na	Al	Mg	Fe	Ca	Lanthanides (La, Ce, Pr, Nd)	others	Si-Al-Na
PG	50	23	13	7	3	1	n.d.	1	2	43%
gel without CBG	49	32	2	9	1.5	1.5	n.d.	2.1	2.9	43%
gel with CBG- (a)	52	30	3.7	9	2	1	n.d.	1	1.3	42.7%
gel with CBG- (b)	50	31	2.7	9	1.5	1.8	1.9	1	1.1	42.7%
ICP with and without CBG	38	0.8	n.d.	n.d.	n.d.	61	n.d.	n.d.	0.2	/

**Table 6: SEM-EDS analyses (wt.%) performed in the precipitated phases present on the gel surface of AVM glass in the system with CBG**

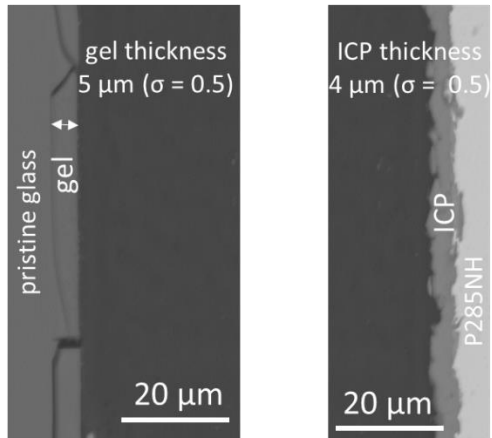
Elements	O	Si	Mg	Al	Ca	Fe	Na
1 (Figure 4-a)	43	32	13	8	2	1.4	0.6
2 (Figure 4-b)	41	25	3.3	5.5	12	13	0.2
3 (Figure 4-b)	43	2.5	1.2	n.d.	40	10	3.3

Table 7: solubility of different minerals of smectites group

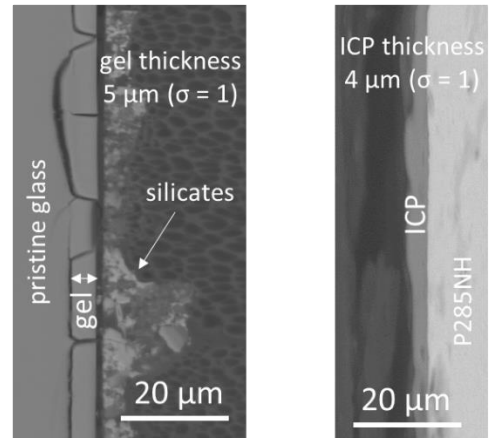
	Mineral	Formula	Log Ks (60°C)	Log Ks (100°C)	Ref.
Smectite group	Saponite	$Mg_{3.165}Al_{0.33}Si_{3.67}O_{10}(OH)_2 + 7.32 H^+ = 3.165 Mg^{2+} + 4.66 H_2O + 0.33 Al^{3+} + 3.67 SiO_{2(aq)}$	22.58	18.72	Bethke et al.[55]
	Montmorillonite	$Fe_{0.175}Mg_{0.35}Al_{1.65}Si_4O_{10}(OH)_2 + 6 H^+ = 0.175 Fe^{2+} + 1.65 Al^{3+} + 4 SiO_{2(aq)} + 4 H_2O + 0.35 Mg^{2+}$	1.51	-1.01	Wilson et al.[56]
	Nontronite	$Mg_{0.165}Fe_2Al_{0.33}Si_{3.67}O_{10}(OH)_2 + 7.32 H^+ = 0.165 Mg^{2+} + 4.66 H_2O + 0.33 Al^{3+} + 3.67 SiO_{2(aq)} + 2 Fe^{2+}$	-12.61	-13.61	Bethke et al.[55]

## Figures

AVM glass/steel interface **without** CBG



AVM glass/steel interface **with** CBG



Graphical abstract

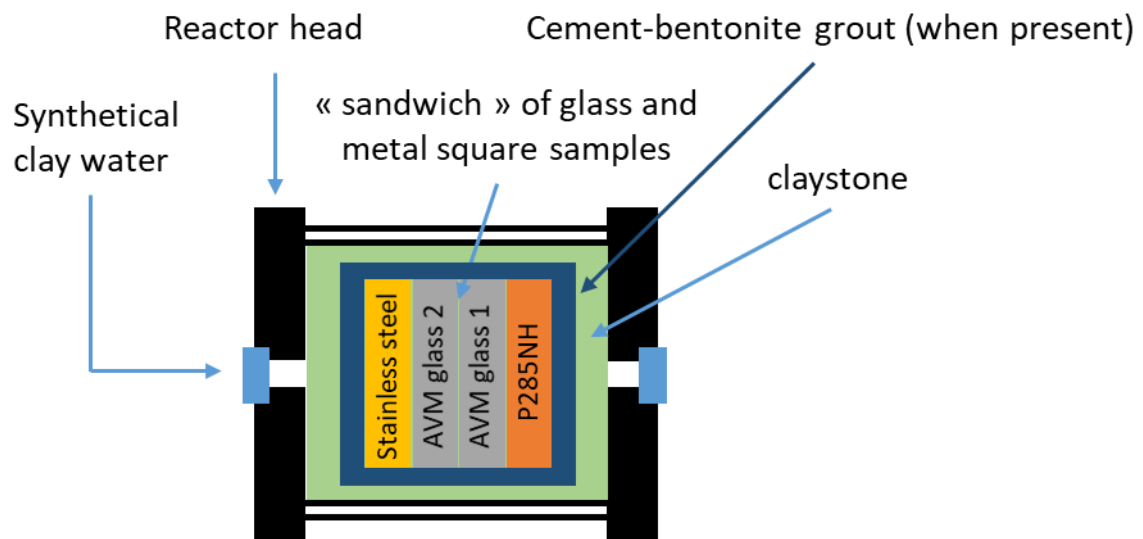


Figure 1: schematic view of the glass/steel/claystone system altered in reactor

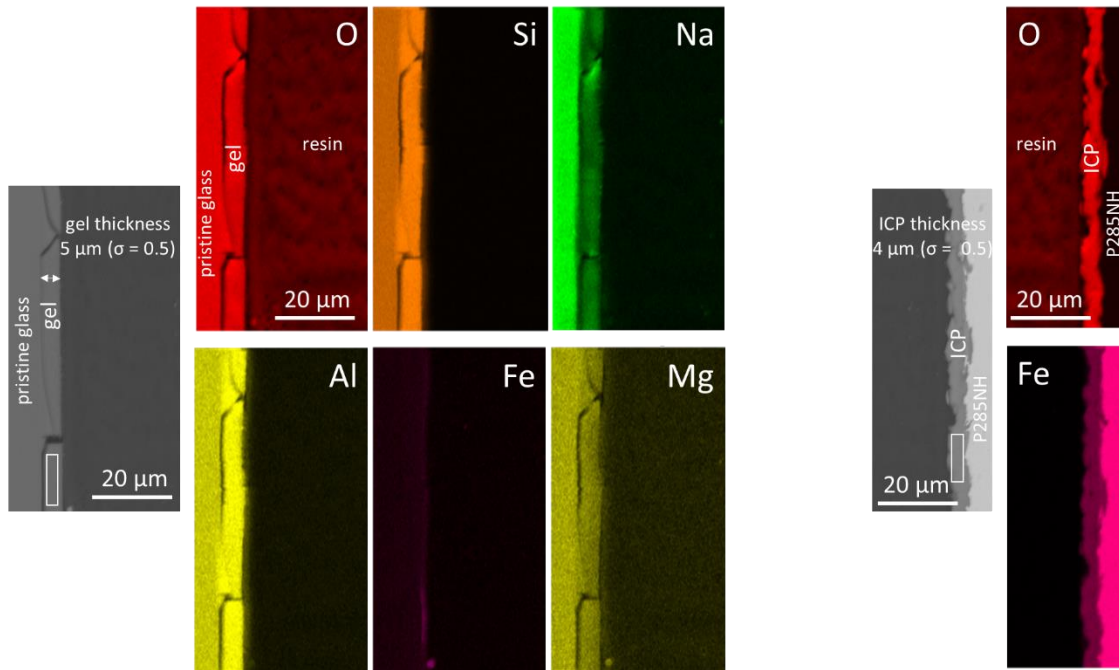


Figure 2: SEM micrograph (backscattered electron) and EDS elementary mapping obtained at the AVM glass/P285NH carbon steel interface without cement-bentonite grout. White rectangle indicates the location of EDS analysis of Table 5 in the gel

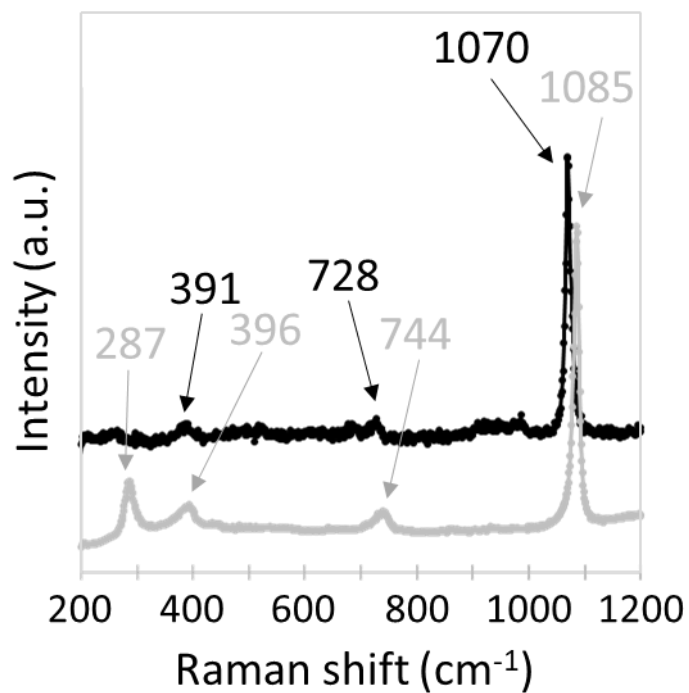


Figure 3: μRaman spectra obtained in the ICP at the AVM glass 1/carbon steel interface without CBG (grey) and with CBG (black) evidencing siderite and chukanovite respectively

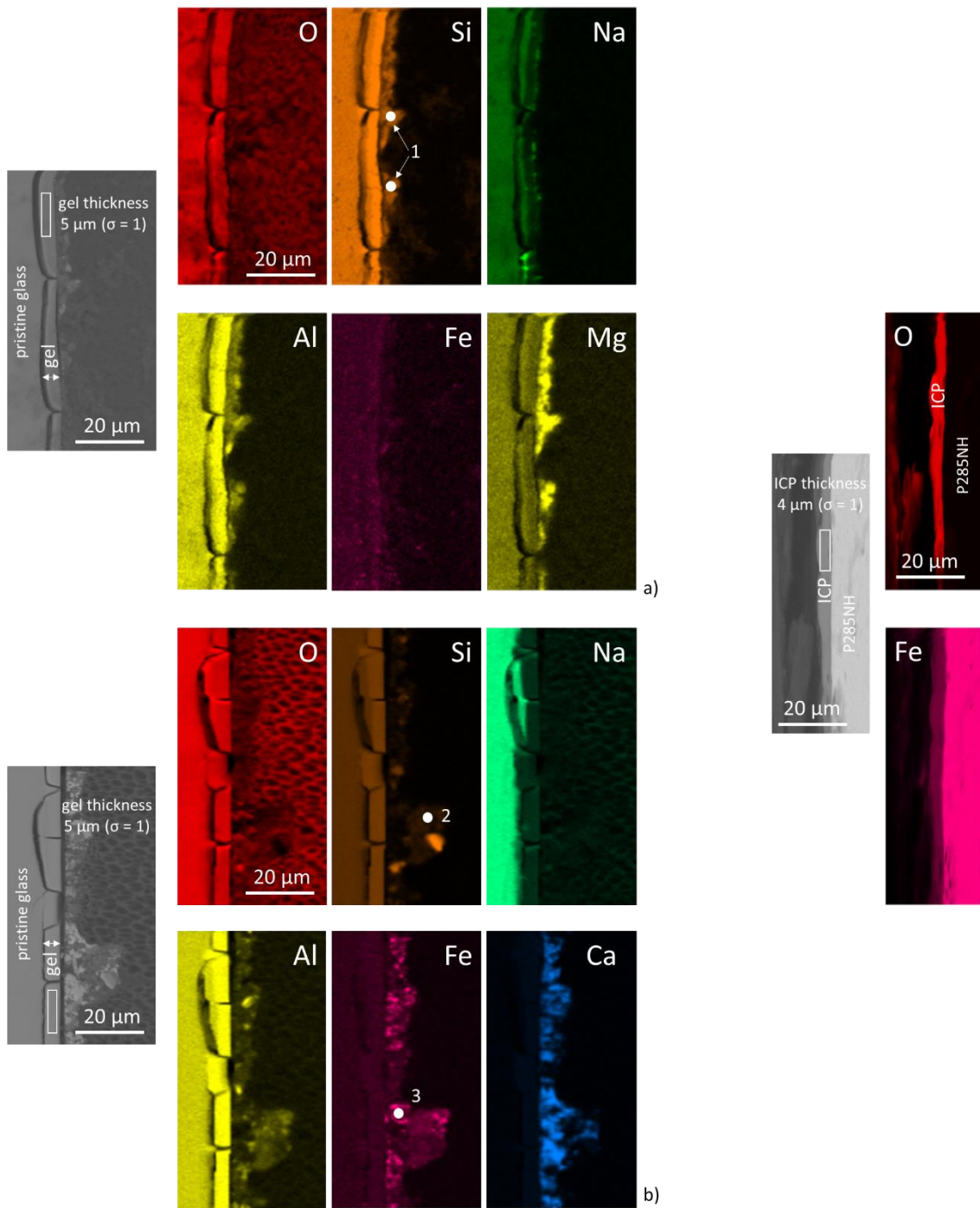


Figure 4: SEM micrograph (backscattered electron) and EDS elementary mapping obtained at the AVM glass/P285NH carbon steel interface with the CBG evidencing silicate on the gel containing (a) Si-Al-Mg phases and (b) Si-Fe-Ca phases. White rectangles and white points indicate the location of EDS analyses of Table 5 and Table 6